








Effect of Gain Saturation on Wideband WDM Signal in PPLN-Based Optical Parametric Amplifier

Shimpei Shimizu , *Member, IEEE*, Takayuki Kobayashi , *Member, IEEE*, Takushi Kazama , Masanori Nakamura , *Member, IEEE*, Akira Kawai , Koji Enbutsu , Takeshi Umeki , *Member, IEEE*, and Yutaka Miyamoto, *Member, IEEE*

Abstract—The periodically poled LiNbO₃ (PPLN) based optical parametric amplifier (OPA) is a technology that contributes to the construction of multi-band wavelength-division multiplexing (WDM) optical networks thanks to its wide amplification bandwidth and wavelength conversion function. In addition, the fast response of the OPA means it is unaffected by sudden changes of wavelength channels due to dynamic channel add-drop. However, such fast response leads to nonlinear signal distortion when operating in the gain saturation region. This paper experimentally investigates the conversion of gain saturation into the nonlinear amplitude distortion in a 64-Gbaud 64QAM WDM signal. We characterized the input power tolerance of a PPLN-based OPA in wideband WDM applications and found that the nonlinear amplitude distortion can be suppressed by increasing the number of WDM channels. For a 75-GHz-spacing 64-channel WDM configuration, the total input power tolerance was improved by ~ 10 dB compared to a single-channel case. We also confirmed that there is almost no wavelength dependence of the effect of gain saturation on the signal distortion. These results show that PPLN-based OPAs have a wide total input power range for amplifying wideband WDM signals in terms of the nonlinear distortion.

Index Terms—Optical fiber communication, optical parametric amplification, wavelength division multiplexing.

I. INTRODUCTION

WIDEBAND wavelength-division multiplexing (WDM) technologies utilizing multi-telecommunication bands are indispensable for further increasing the capacity of optical fiber networks [1], [2], [3], [4]. Optical amplifiers have been utilized in these networks to compensate for the fiber-propagation loss, and erbium-doped fiber amplifiers (EDFAs), which have

an amplification bandwidth of ~ 4 THz in the C- or L-bands, are currently being used. For constructing high-capacity multi-band WDM networks using C-, L-, and other bands, a wideband optical amplification technology is essential. In addition, getting optical devices such as transponders and wavelength-selective switches to apply to additional bands is required.

An optical parametric amplifier (OPA) utilizing nonlinear optical effects can potentially obtain a broader amplification bandwidth than conventional EDFAs. For example, periodically poled LiNbO₃ (PPLN) waveguides or highly nonlinear fibers (HNLFs) used as amplification media have obtained the wide gain bandwidth of > 10 THz [5], [6]. In addition, by customizing the phase-matching characteristics of the amplification medium and pump allocation, the amplification band can be applied to various telecommunication bands [7], [8]. Especially, as the PPLN-based OPA produces relatively few unwanted nonlinear optical effects among WDM channels, it is suitable for amplifying a wideband WDM signal with a high gain. Inline-amplified transmission of a wideband WDM signal using the PPLN-based OPA has been demonstrated, including a 5.125-THz inline-amplified transmission over 3×30 km with a 41-channel 800-Gbps/ λ WDM signal [9]. The PPLN-based OPA has also been combined with a forward-pumped distributed Raman amplification and demonstrated a 6.25-THz inline-amplified transmission over 3×80 km with a 50-channel 1-Tbps/ λ WDM signal [10]. These demonstrations utilized one side of the gain bandwidth of the OPA, and therefore, showed the potential for inline-amplified transmission using OPA repeaters over 10 THz. Another function of OPAs is wavelength conversion performing by utilizing the phase-conjugated copy, namely idler light, generated with signal amplification. The simultaneous wavelength conversion between telecommunication bands allows existing optical components for conventional bands to be used for new bands [11], [12], [13], [14], [15]. Configurations that apply an OPA-based wavelength converter to S-band amplifier [11], multi-band Tx/Rx [12], [13], [14], and optical cross-connect [15] have been demonstrated. In addition, the ultrafast response of nonlinear optical effects at the femtosecond scale [16] enables the OPA to cope with sudden changes in input power due to dynamic channel add-drop [9]. For these reasons, the OPA is a promising technology for contributing to the construction of future multi-band optical networks.

Gain saturation is a key characteristic of OPAs for optical communication applications. In a slow-response amplifier such

Manuscript received 15 December 2022; revised 31 January 2023 and 21 February 2023; accepted 24 February 2023. Date of publication 1 March 2023; date of current version 2 August 2023. (*Corresponding author: Shimpei Shimizu.*)

Shimpei Shimizu, Takayuki Kobayashi, Masanori Nakamura, Akira Kawai, and Yutaka Miyamoto are with the NTT Network Innovation Laboratories, NTT Corporation, Yokosuka 239-0847, Japan (e-mail: shimpei.shimizu.ge@hco.ntt.co.jp; takayuki.kobayashi.wt@hco.ntt.co.jp; masanori.nakamura.cu@hco.ntt.co.jp; akira.kawai.ku@hco.ntt.co.jp; yutaka.miyamoto.fb@hco.ntt.co.jp).

Takushi Kazama and Takeshi Umeki are with the NTT Network Innovation Laboratories, NTT Corporation, Yokosuka 239-0847, Japan, and also with the NTT Device Technology Laboratories, NTT Corporation, Atsugi 243-0198, Japan (e-mail: takushi.kazama.me@hco.ntt.co.jp; takeshi.umeki.zv@hco.ntt.co.jp).

Koji Enbutsu is with the NTT Device Technology Laboratories, NTT Corporation, Atsugi 243-0198, Japan (e-mail: koji.enbutsu.cm@hco.ntt.co.jp).

Color versions of one or more figures in this article are available at <https://doi.org/10.1109/JLT.2023.3250823>.

Digital Object Identifier 10.1109/JLT.2023.3250823

as an EDFA, the gain saturation only limits the output power, and the input signal light is amplified linearly even when operated in the gain saturation region. In contrast, the gain saturation of the OPA not only limits the output power but also causes nonlinearity of the gain that depends on the input time waveform due to an ultrafast response of nonlinear optical effects at the femtosecond scale which is much shorter than the symbol period. For the signals modulated without multi-levels in the amplitude direction (e.g., OOK and BPSK), the gain nonlinearity can be utilized for suppression of the amplitude noise [17], [18]. For multi-level signals, however, it has been suggested that the gain nonlinearity may lead to nonlinear signal distortion [19]. A similar nonlinear distortion has been extensively studied both experimentally and analytically in semiconductor optical amplifiers (SOAs) [20], [21], [22], [23], where nonlinear phase and amplitude distortions occur in narrow-bandwidth signals due to sub-nanosecond carrier lifetime. The nonlinear distortion in the SOA can be suppressed when the bandwidth of the input signal is increased with a high-symbol rate and WDM. While the gain saturation of OPAs has been extensively studied in terms of the I/O power relation and amplitude noise characteristics [17], [18], [24], [25], [26], [27], [28], its effect on the distortion of wideband and spectral-efficient coherent signals (e.g., higher-order QAM) has not been fully investigated. How the gain saturation in OPAs with a fast response time distorts wavelength-multiplexed higher-order QAM signals will be an important insight in determining the I/O power operation range for applying OPAs in optical networks.

In this paper, we experimentally investigate the effect of the gain saturation in a polarization-diverse PPLN-based OPA on signal quality for wideband WDM applications. A 75-GHz-spaced 64-Gbaud dual-polarization (DP-) 64QAM WDM signal over 4.8 THz was utilized as the test signal for our experiments. The PPLN-based OPA we used has a center wavelength of 1572.89 nm in the amplification band and can also be used as a wavelength-band converter between C- and L-bands. We found that nonlinear distortion can be reduced by utilizing the wideband WDM signal. In Section II, we describe the fundamental configuration of our polarization-diverse PPLN-based OPA. In Section III, the gain saturation characteristics as an I/O power relation in single-channel and WDM cases are shown. In Section IV, the nonlinear signal distortion induced by the gain saturation in a single-channel case is characterized with a peak to average power ratio (PAPR) changed by chromatic dispersion (CD). In Section V, we investigate the nonlinear signal distortion in WDM configurations. The differences between the WDM case and single-channel case and demonstrate that increasing the number of channels is effective for suppressing the nonlinear distortion.

II. CONFIGURATION OF PPLN-BASED OPA

This section describes the configuration of the polarization-diverse PPLN-based OPA used in our experiments and its basic performance with a small signal approximation. Fig. 1 shows its configuration when used as (a) a wideband inline amplifier and (b) a wavelength converter. Since the output of the OPA contains both signal and idler light, it is necessary to reject either band

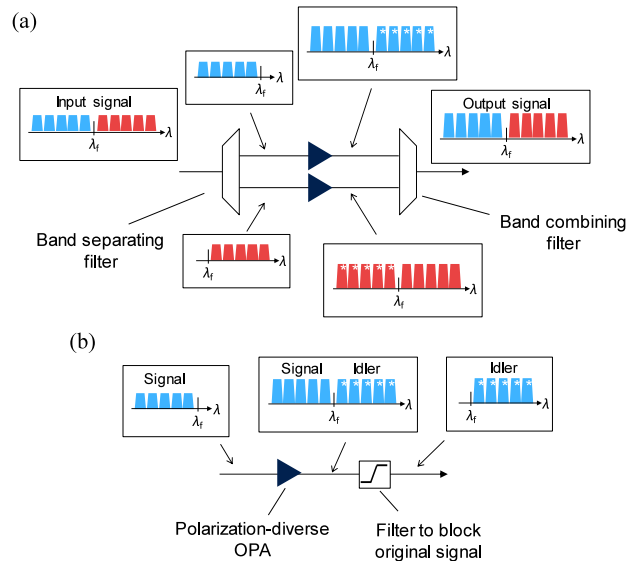


Fig. 1. Configurations of OPA applications for wideband WDM transmission, where λ_f is center wavelength of amplification band. (a) Wideband inline amplification. (b) Wavelength band conversion.

using an optical filter; the band of the original signal is rejected when the OPA is used as a wavelength converter. To fully utilize the wide gain bandwidth of the OPA, it is necessary to separate the input signal into two bands and amplify them independently [29], [30], [31], as shown in Fig. 1(a). When separating into two bands at the input side of the OPA, if the extinction ratio of the band-separating filter is not sufficient, interference between the channels can occur during the optical parametric amplification process. When the OPA is operated with high amplification gain, the idler light is generated at almost the same level as the signal light, so the band-combining filter must also have a high extinction ratio between the signal and idler. If these extinction ratios are not sufficient, additional band blockers may be required. On the other hand, since the optical parametric amplification process has polarization dependence, regardless of whether it is $\chi^{(3)}$ -based or $\chi^{(2)}$ -based, polarization-diverse configurations that process each orthogonal polarization component of the signal light independently are often used. Among the several types of polarization-diverse OPA have been proposed [32], [33], [34], we opted to use the parallel type [9], [35] in this study. Note that only one side of the OPA bandwidth is used in our experiments.

Fig. 2 shows the configuration of the polarization-diverse PPLN-based OPA we used in our experiments. First, the signal light was separated into two orthogonal polarization components using a polarization-beam splitter (PBS) for polarization independent amplification. Two PPLN waveguides per polarization were used: one for optical parametric amplification of the signal light (PPLN1 and 2) and the other for conversion of the pump light (PPLN3 and 4) into second-harmonic (SH) light. The wavelength of the pump light used in the $\chi^{(2)}$ -based OPA is one half of λ_f , which is the center wavelength of the phase-matching band (gain band) of the OPA medium. For obtaining the high-power pump light, a pump light source at λ_f , which is an external cavity laser (ECL) with a ~ 30 -kHz linewidth, was used, along with EDFAs. The pump light at λ_f was split into two for each polarization

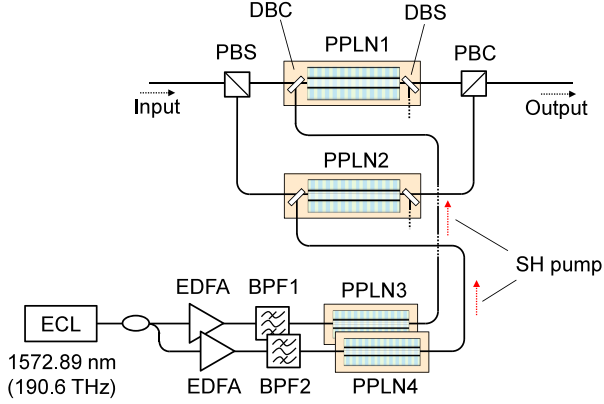


Fig. 2. Configuration of parallel-type polarization-diverse PPLN-based OPA with $\lambda_f = 1572.89$ nm. PBS/PBC: polarization-beam splitter/combiner, DBS: dichroic beam splitter, DBC: dichroic beam combiner, ECL: external cavity laser, BPF: band-pass filter.

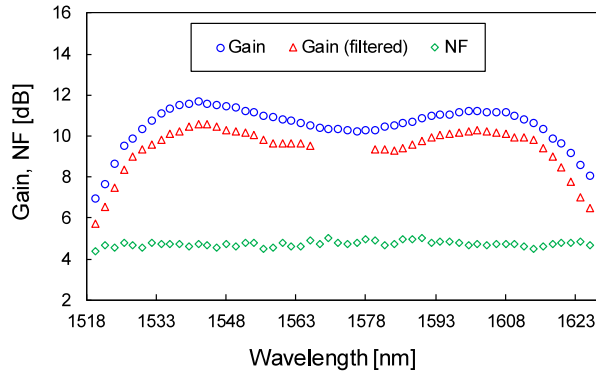


Fig. 3. Gain and NF spectrum of polarization-diverse PPLN-based OPA measured by wavelength sweep of input CW light.

signal component, amplified by EDFAs, and then converted into SH light with a second-harmonic generation (SHG) process in PPLN3 and 4. The signal light was combined and decombined with the SH pump light using a dichroic beam combiner and splitter (DBC/DBS) at the input and output of PPLN1 and 2. We utilized a 4-port PPLN module implementing PPLN1 and 2 to integrate the DBC/DBS and each waveguide, thereby achieving low-loss (de-)combining of the signal and SH pump light [36], [37]. The center wavelength of the phase-matching of the PPLN waveguides was 1572.89 nm at the border between the C- and L-bands. By performing SHG and OPA in different media, parametric cross-talk (PXT) caused by unwanted wavelength conversion can be suppressed [38].

We measured the gain and NF spectra of the polarization-diverse PPLN-based OPA for the small signal, that is, in unsaturated region. The waveguide temperature and optical power of the SH pump were adjusted so that the OPA had a 5.3-THz 10-dB-gain bandwidth. The 5.3-THz bandwidth was necessary to amplify a 4.8-THz WDM signal, including the guard band of 0.5 THz for filtering the idler light. Fig. 3 shows the gain and noise figure (NF) spectra of the polarization-diverse PPLN-based OPA with ~ 10 -dB gain operation. The gain after filtering the idler light is also shown. The spectra were measured by

sweeping the wavelength of input CW light at -25 -dBm input power, and the NF was calculated with an optical spectrum analyzer (OSA) [39]. The NF spectrum was flat, and the maximum value was 5.1 dB. When the waveguide temperature was detuned so that the gain spectrum was wideband, a gradient in the gain spectrum was created due to a decrease in gain around λ_f .

III. GAIN SATURATION AS I/O POWER RELATION

This section describes the I/O power relation of our polarization-diverse PPLN-based OPA for a wideband WDM signal. The 64-channel 64-Gbaud WDM signal is implemented with 75-GHz spacing over 4.8 THz.

A. Gain Saturation in $\chi^{(2)}$ -Based OPA

The coupled wave equation (CWE) of the $\chi^{(2)}$ -based optical parametric amplification process within the PPLN waveguide is given as [40]

$$\frac{dA_s(z)}{dz} = -\frac{\alpha_s}{2} A_s(z) + j\kappa_s A_p(z) A_i^*(z) \exp(j\Delta\beta z), \quad (1)$$

$$\frac{dA_i(z)}{dz} = -\frac{\alpha_i}{2} A_i(z) + j\kappa_i A_p(z) A_s^*(z) \exp(j\Delta\beta z), \quad (2)$$

$$\frac{dA_p(z)}{dz} = -\frac{\alpha_p}{2} A_p(z) + j\kappa_p A_s(z) A_i(z) \exp(-j\Delta\beta z), \quad (3)$$

where A_s , A_i , and A_p are the complex amplitudes of signal, idler, and pump light, α is the absorption coefficient of each light in the PPLN waveguide, and κ is the efficiency of each light in the PPLN waveguide. The amount of a phase mismatch between signal, idler, and pump light, $\Delta\beta$, is expressed as [41]

$$\Delta\beta = \frac{1}{c} (n_p \omega_p - n_s \omega_s - n_i \omega_i) - \frac{2\pi}{\Lambda}, \quad (4)$$

where Λ is the poling period of the PPLN waveguide, c is the speed of light, and n_s , n_i , and n_p indicate the refractive index of the PPLN waveguide at frequencies of the signal, idler, and pump light, respectively. The relation between each frequency is $\omega_s = \omega_p - \omega_i$. If the pump light is sufficiently stronger than the signal light (without pump depletion), the following analytical solution is given for the amplification gain:

$$G_s = \cosh^2(gL) + \left(\frac{\Delta\beta}{2g}\right)^2 \sinh^2(gL), \quad (5)$$

$$g \equiv \sqrt{\kappa^2 P_p - \left(\frac{\Delta\beta}{2}\right)^2}, \quad (6)$$

where P_p is the input power of the pump light and L is the length of the PPLN waveguide. Note that, we approximated $\kappa = \kappa_s = \kappa_i = \kappa_p/2$ and assumed no optical absorption in the waveguide ($\alpha = 0$). The reason for the slope in the gain spectrum (as shown in Fig. 3) is that $\Delta\beta$ is not uniform. The frequency dependence of $\Delta\beta$ is determined by that of the refractive index, which in turn depends on waveguide temperature [42]. Thus,

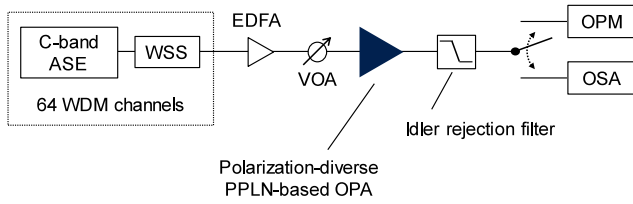


Fig. 4. Experimental setup for measurement of I/O power characteristics. WSS: wavelength-selective switch, VOA: variable optical attenuator, OPM: optical power meter, OSA: optical spectrum analyzer.

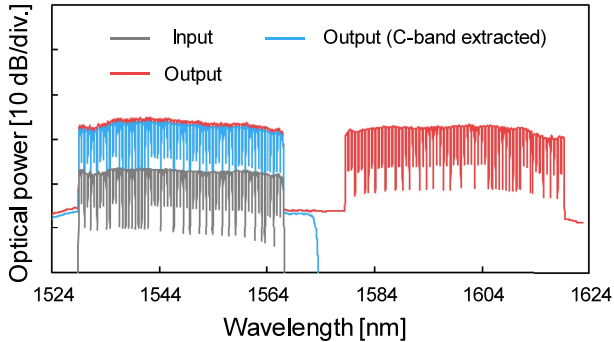


Fig. 5. Input and output spectra of polarization-diverse PPLN-based OPA in 75-GHz-spaced 64-channel case (0.1-nm resolution).

the form of the gain spectrum also depends on the waveguide temperature [5]. With the large input power of the signal light, gain saturation occurs due to pump depletion. The saturated gain cannot be expressed with an analytical solution, so numerical simulation or experimental measurement is required for evaluating the saturated gain of OPAs. Therefore, before evaluating signal distortion, we experimentally measured the I/O power characteristics of our PPLN-based OPAs used in this study.

B. Results of I/O Power Measurement

Fig. 4 shows the experimental setup for the evaluation of gain saturation in the polarization-diverse PPLN-based OPA with a wideband WDM signal. The WDM signal was emulated using C-band amplified spontaneous emission (ASE) light output from an EDFA and a wavelength-selective switch (WSS). The WSS shaped the ASE light into a spectrum to mimic a 75-GHz-spaced 64-Gbaud WDM signal. The ASE light was unpolarized and input equally to each polarization diversity path. The total input power of the signal to OPA was adjusted with an EDFA and a variable optical attenuator (VOA). Fig. 5 shows the input and output spectra of the 64-channel WDM signal measured with an OSA. The gradient of the input spectrum was flattened to within 2 dB. The non-uniformity of the notch level in the measured WDM signal was due to the resolution and sampling points of the OSA. After the OPA, the amplified WDM signal passed through an idler rejection filter, and the amplified C-band signal was extracted. We measured the optical power of the extracted WDM signal using an optical power meter (OPM). The gain was measured in both the single-channel case and 64-channel WDM case. The signal bandwidth was 64 GHz (centered at

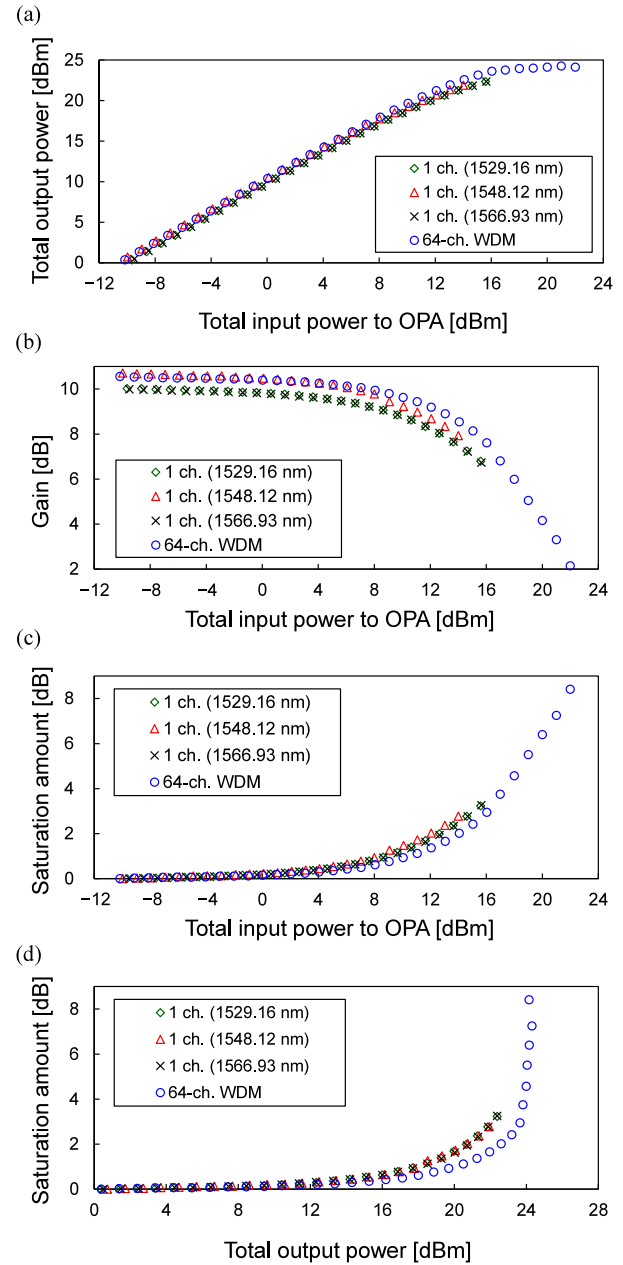


Fig. 6. Gain saturation characteristics of polarization-diverse PPLN-based OPA. (a) I/O power relation. (b) Gain characteristics. (c) Gain-saturation amount with total input power. (d) Gain-saturation amount with total output power.

1529.16, 1548.12, and 1566.93 nm) in the single-channel case and 4.8 THz in the 64-channel case.

Fig. 6 shows the measured gain characteristics in each case. The gain-saturation amount was calculated based on the gain at -10 -dBm input. As we can see, the I/O power relation was linear in the low input power region, but saturated at the output power of ~ 24 dBm in the high input power region. That is, the gain decreased as the input power increased, as shown in Fig. 6(b). Meanwhile, in the single-channel case, the gain saturation with respect to the input power shown in Fig. 6(c) was slightly suppressed at wavelengths with smaller gain (1529.16 and 1566.93 nm) than that at a wavelength with

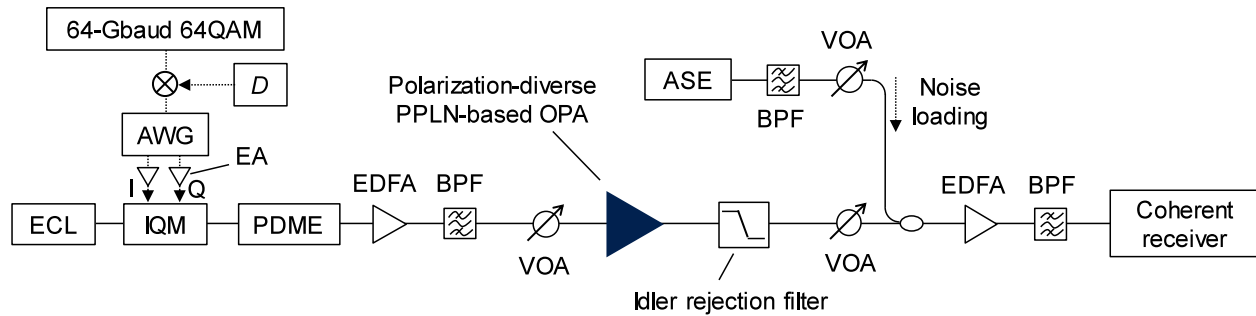


Fig. 7. Experimental setup for 75-GHz-spaced 64-channel WDM signal amplification. ECL: external cavity laser, EA: electrical amplifier, AWG: arbitrary waveform generator, IQM: I/Q modulator, D : chromatic dispersion added to electrical signal data within Tx DSP, PDME: polarization-division-multiplexing emulator, BPF: band-pass filter, VOA: variable optical attenuator.

higher gain (1548.12 nm). However, Fig. 6(d), which plots gain saturation versus output power, shows the almost same results for all single-channel cases. This means that the gain saturation in the PPLN-based OPA is characterized by the output power regardless of the wavelength. Prior studies have reported that in $\chi^{(3)}$ -based optical parametric amplification (e.g., fiber-based OPA), significant wavelength dependence of gain saturation occurs due to self- and cross-phase modulation of the pump, signal, and idler light [24] and dispersion slope [26]. However, in $\chi^{(2)}$ -based optical parametric amplification, the phase-matching characteristics depend almost exclusively on refractive index of the media, as shown in (4). Therefore, the gain saturation with respect to the output power of the PPLN-based OPA did not depend on the wavelength in the single-channel case.

Gain saturation in a WDM signal is caused by the consumption of a single pump light for amplification of wideband signals and idlers, and we found here that the gain saturation of the WDM signal was relaxed by ~ 1.5 dB compared to the single-channel signal. In the optical parametric amplification process, as the power of signal-idler pairs increases, the energy transfer from the pairs to the pump occurs in the opposite direction to the process by which the signal is amplified [24], [27]. This is caused by the sum-frequency generation process between the signal-idler pairs in $\chi^{(2)}$ -based media. The evolution of this process is wavelength dependent since it depends on the gain (phase-matching condition) of each frequency component. Under WDM conditions, the signal power is spread over various frequency components. Therefore, the complex pump power dynamics via interactions between different signal-idler pairs would contribute to a slight relaxation of the gain saturation characteristics for the average power of the WDM signal. Despite such slight difference between the single-channel and WDM cases, the trends were in good agreement in both cases.

IV. SIGNAL DISTORTION CHARACTERISTICS IN SINGLE CHANNEL AMPLIFICATION

First, we attempted to characterize the distortion of the single-channel signal in terms of the PAPR of the signal time waveform. Because the response time of the OPA is very fast, the high PAPR signal is considered to result in a larger distortion at a large power timing compared to the low PAPR signal even at the

same average input power. CD is one factor that can change the PAPR [43]. Therefore, we added CD to the signal in the transmitter-side digital signal processing (DSP) to investigate the signal distortion induced by the gain saturation.

Fig. 7 shows the experimental setup. The wavelengths of the channel under test (CUT) were set to 1529.16 nm, 1548.12 nm, and 1566.63 nm corresponding to ch. 1, ch. 32, and ch. 64 of the 64-channel WDM configuration, respectively. The modulation format was Nyquist-pulse-shaped 64-Gbaud uniform DP-64QAM with a 0.03-roll-off factor. The tested signal pattern was randomly generated, and its unique length was 102400 symbols. An arbitrary CD was given to the signal data within the DSP on the transmitter side. The CW light at the wavelength of the CUT from an ECL was modulated with the electrical signal output from an arbitrary waveform generator (AWG) using an I/Q modulator (IQM). After optical modulation, the CUT was polarization-multiplexed by passing through a polarization-division-multiplexing emulator (PDME) with a 15-m delay between X- and Y-components. The input power of the CUT to the PPLN-based OPA was then adjusted with an EDFA and VOA. The PPLN-based OPA with a parallel-type polarization-diverse configuration amplified the CUT and generated its idler. The idler component was rejected with an idler rejection filter. Before coherent reception, the OSNR of the CUT was adjusted to 30 dB by loading the ASE noise from an EDFA into the signal band. The CUT was received by a dual-polarization coherent receiver with four 70-GHz balanced photodetectors. The received signal was digitized using a 256-Gsample/s digital storage oscilloscope and demodulated with offline DSP on the basis of a complex 8×2 adaptive equalizer (AEQ) in the frequency domain [44]. The signal was received over 6M samples. Before the AEQ, the signal data was resampled to 2 samples/symbol, and then, a frequency-domain fixed equalizer (FEQ) compensated for the CD. The fast Fourier transform (FFT) block size in the FEQ was the entire sample. The block size of the FFT in the frequency-domain AEQ was 1024 samples, which was large enough to eliminate the penalty due to CD even if CD remained after the FEQ operation. The AEQ was driven by the decision-directed algorithm and the pilot-aided algorithm using periodically inserted pilot symbols. The SNR of the signal qualities was calculated on the basis of the variance of the signal from desired symbols. We also evaluated signal quality at normalized generalized mutual

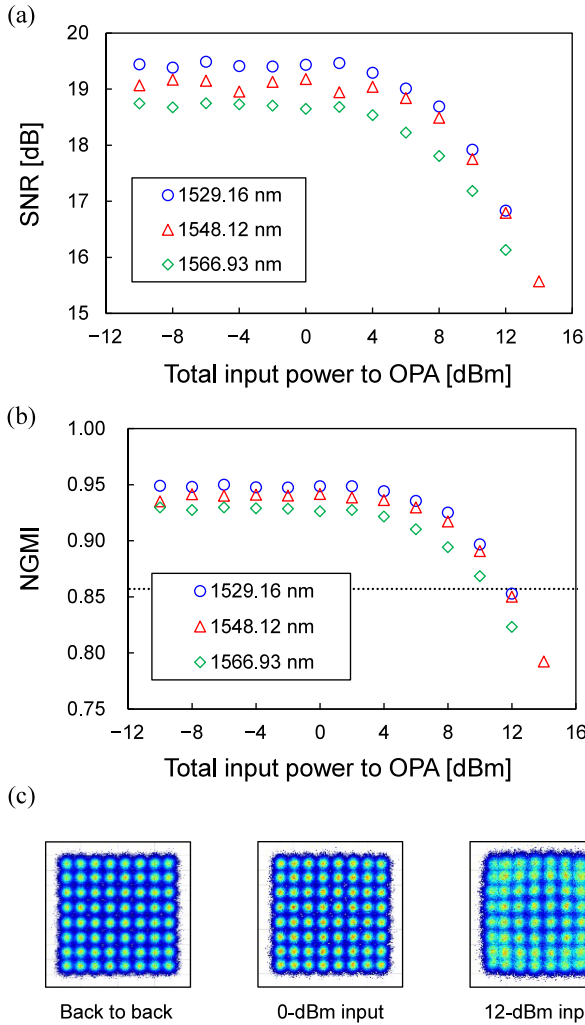


Fig. 8. Input power characteristics of signal distortion induced by gain saturation of OPA in single-channel amplification with zero-dispersion condition. (a) SNR characteristics. (b) NGMI characteristics. Dashed line is NGMI threshold for 624 Gbps/ λ . (c) Constellations of demodulated signal at 1548.12 nm.

information (NGMI). Assuming the concatenated coding of low-density parity-check code and BCH code with a code rate of 0.826 and a 1.64% pilot symbol inserted in the signal data, the net data rate was 624 Gbps/ λ with the NGMI threshold of 0.857 [9].

Fig. 8 shows the input power characteristics of the signal quality under the zero-CD condition. SNR and NGMI degradation were correlated. Degradation of signal quality was observed around 4-dBm input at each wavelength. At 12-dBm input, ~ 2.5 -dB SNR degradation was observed, and all channels were below the NGMI threshold. The input power for a 1-dB SNR penalty was 8 dBm with a gain reduction of 0.9 dB. As expected from the measured I/O power relationship shown in Fig. 6, the wavelength dependence of the SNR degradation was small, and the $\chi^{(2)}$ -based OPAs maintained flat wavelength characteristics even when operated in the gain-saturated region. In constellation diagrams, the nonlinear distortion was not clearly observed in the unsaturated region of 0-dBm input, but in the gain-saturated region of 12-dBm input, clear nonlinear distortion was observed.

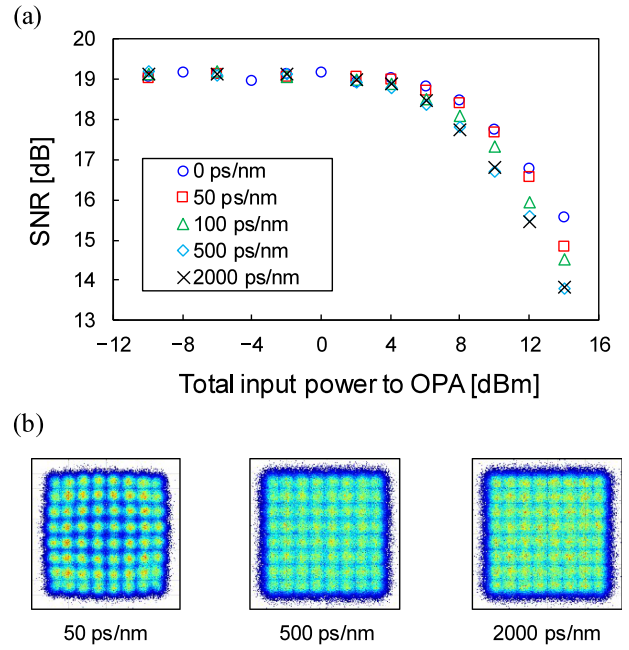


Fig. 9. Chromatic dispersion dependence of input power characteristics at 1548.12 nm. (a) SNR characteristics. (c) Constellations at 12-dBm input.

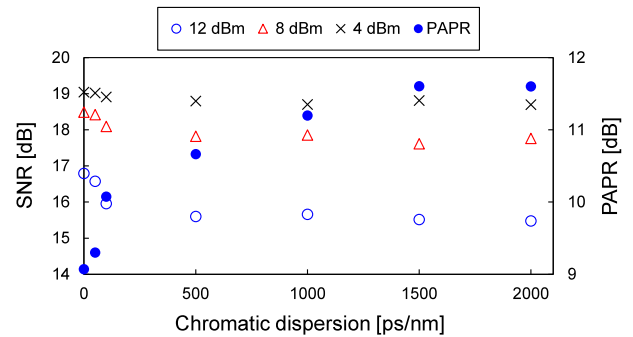


Fig. 10. CD dependence of signal distortion in 4-dBm, 8-dBm, and 12-dBm input cases and calculated PAPR of each dispersed signal.

The gain saturation induced the distortion of amplitude direction according to the power of each symbol point, and thus, large-power symbols were strongly distorted. Although nonlinear phase noise also occurred in the gain-saturated SOA [20], the gain-saturated PPLN-based OPA caused only amplitude noise.

Next, we tested the signals under the condition with CD. The wavelength of the CUT was 1548.12 nm. Fig. 9 shows the experimental results, where we can see that signal distortion increased as CD increased, and the results for 500 ps/nm and 2000 ps/nm were almost identical. The results in the unsaturated region confirm that there was no penalty for adding the CD. In the constellations, a clear nonlinear amplitude distortion was visible at 50 ps/nm. However, at 500 ps/nm and 2000 ps/nm, the distortion due to gain saturation was distributed in all symbols, not just in symbols with large amplitude values. The reason for this is presumably the spread of symbols due to the CD. Fig. 10 shows the CD dependence of the signal distortion at each input power and calculated PAPR of signals. We can see that the

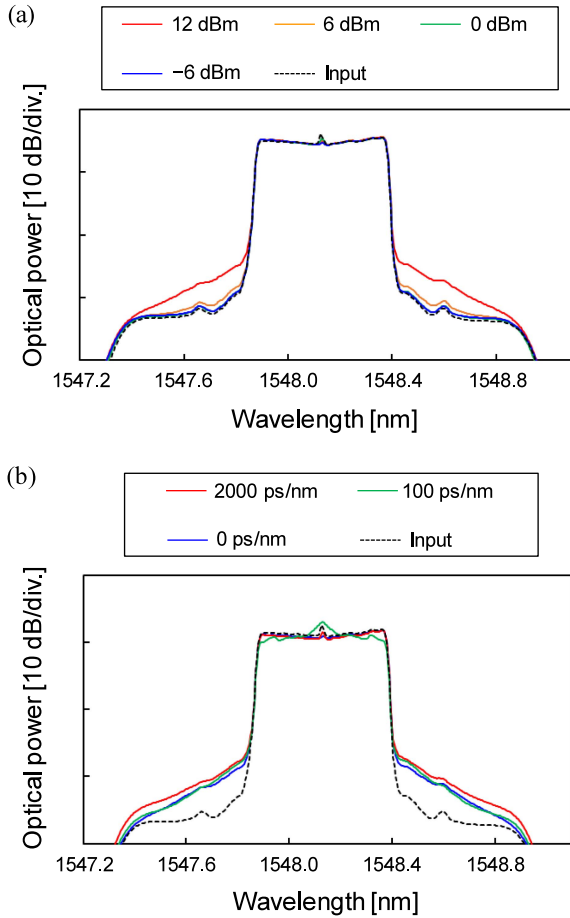


Fig. 11. Optical spectra of amplified signal at 1548.12 nm. (a) Zero-dispersion case. (b) Each dispersion case at 12-dBm input.

signal distortion varied greatly in the range up to ~ 100 ps/nm, increased slowly up to ~ 500 ps/nm, and saturated at higher CD. The PAPR also showed a similar trend, increasing as the signal quality degraded. The PAPR increased slowly above 500 ps/nm, but its effect on signal quality was not observed to be significant. This indicates that the effect of PAPR saturates above a certain amount because the appearance of large peaks in the high-CD region was actually rare. The finite unique length of the signal used in the experiment may also have contributed to the difficulty in observing changes of signal quality in the high-CD region. These results demonstrate that, for single-channel amplification, the nonlinear signal distortion induced by the gain saturation of the OPA can be characterized by PAPR.

Fig. 11 depicts the amplified spectra of the CUT at 1548.12 nm. In the zero-dispersion cases shown in Fig. 11(a), at an input power of -6 dBm, the amplified spectrum matched the input spectrum, but the spectrum of the signal broadened as the input power increased. This phenomenon is similar to the broadening of the signal spectrum caused by self-phase modulation [45], and indicates a nonlinear response of the OPA caused by the gain saturation. Fig. 11(b) shows the dispersed signal cases at 12-dBm input. The spectrum at 100 ps/nm was subject to ripple due to the pattern-dependent waveform change stemming from the CD and the clipping characteristics of the

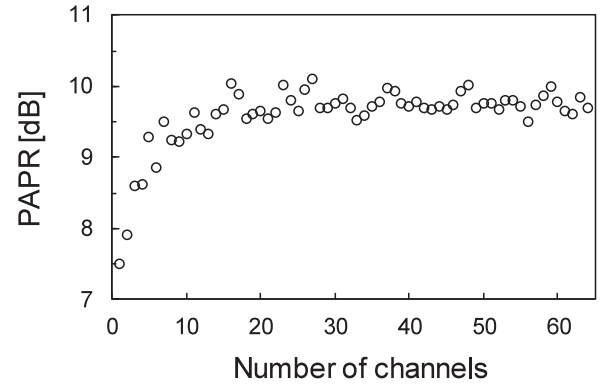


Fig. 12. Calculation example of dependence of PAPR on the number of channels.

AWG related to the increased PAPR of the electrical signal. In fact, this ripple existed before the signal passed through the OPA. When the CD was sufficiently large at 2000 ps/nm, these effects were averaged out and were no longer observed on the optical spectrum. The spectrum at 100 ps/nm was slightly broader than the spectrum at 0 ps/nm, and a broadening of the spectrum at 2000 ps/nm was evident. These results are reasonable in terms of the measured signal quality.

V. CHARACTERIZATION OF SIGNAL DISTORTION IN WDM CONFIGURATION

In the single-channel experiments, we demonstrated that the signal distortion induced by gain saturation can be characterized by the PAPR of the input signal and spectral broadening. As with the addition of CD, WDM causes the PAPR of the signal power to increase. Meanwhile, the contribution of the input power to the OPA of one channel is relatively small in a WDM configuration. Therefore, the effect of gain saturation on the WDM signal will be different from that on a single channel. In this section, we experimentally investigate the nonlinear response of OPA to a WDM signal for wideband WDM applications.

We performed a numerical simulation to estimate the change in PAPR due to WDM. As in the experiment, the signal was calculated with a Nyquist-pulse-shaped 64-Gbaud uniform DP-64QAM with a 0.03-roll-off factor. The signal data of each channel was generated by independently random symbols of the unique length of 100000 symbols per polarization. The electrical field of the WDM signal per polarization was calculated as

$$E_{\text{WDM}}(t) = \sum_n E_n(t) \exp(j2\pi n \Delta f t), \quad (7)$$

$$n = \begin{cases} -\frac{N}{2}, \dots, -1, 0, 1, \dots, \frac{N}{2} - 1 & (N = \text{odd}) \\ -\frac{N-1}{2}, \dots, -1, 0, 1, \dots, \frac{N-1}{2} & (N = \text{even}) \end{cases}, \quad (8)$$

where $E_n(t)$ is the electrical field of each channel, Δf is the channel spacing, n is the channel index, and N is the number of channels. The PAPR was calculated using the sum of the power of two polarizations. Fig. 12 shows a calculation result of the dependence of PAPR on the number of WDM channels. As we

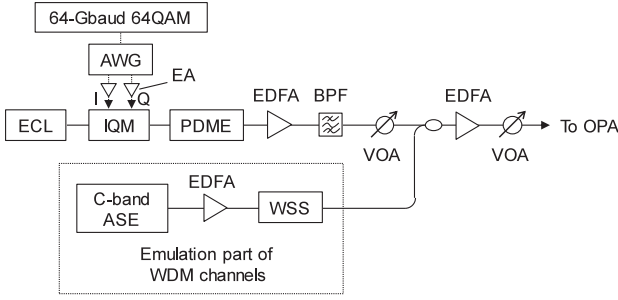


Fig. 13. Transmitter configuration for WDM experiments.

can see, the PAPR of the WDM signal tended to increase as the number of channels increased. This is because the addition of uncorrelated signal series caused the waveform of the WDM signal to approach a Gaussian shape with a large PAPR. This is the same phenomenon that occurs in optical frequency-division multiplexing (OFDM), where PAPR increases when the number of OFDM carriers is increased [46]. The increase of PAPR saturated after 20 channels in our simulation. This is because the peaks of all channels coming at the same time became rarer as the number of channels increased and could not be observed with finite data length. In addition, the plot was not smooth due to the finite data length. Since it was difficult to generate 64 uncorrelated WDM channels in our experiments, we utilized ASE to generate them as in Section III, except for the CUT. Note that, because the time waveform of channels generated from ASE is Gaussian-like, the PAPR of each channel is larger than that of a modulated channel. Therefore, the effects of gain saturation may be slightly overestimated compared to using independently modulated WDM channels, especially when the number of channels is small.

Fig. 13 shows the transmitter configuration for the WDM experiments. The interference WDM channels were emulated using the ASE and the WSS, the same as the setup in Fig. 4. The assumed WDM configuration was a 75-GHz-spacing 64-Gbaud signal, as in the previous sections. The WSS rectangularly hollowed out the ASE at a wavelength of the CUT with 75-GHz bandwidth, and the CUT modulated with 64QAM was inserted into the hollowed-out band. The bandwidth of the WDM signal was up to 4.8 THz within 1529.16–1566.93 nm (64 channels). The setup after the transmitter was the same as in Fig. 7, and the CUT was received with OSNR = 30 dB.

Fig. 14 shows the demodulation results of ch. 1 (1529.16 nm), ch. 32 (1548.12 nm), and ch. 64 (1566.93 nm) with the 64-channel WDM configuration and ch. 16 (1548.12 nm) in the 32-channel WDM configuration. When the signal was multiplexed, we had expected the PAPR to increase because the total waveform of the WDM signal becomes Gaussian-like due to the addition of the various waveforms as shown in Fig. 12. However, no clear signal distortion was seen in the SNR, NGMI, or constellation results in the WDM cases, even at the 12-dBm total input. At input powers above 12 dBm, the signal quality degraded gradually in both WDM cases. For a 1-dB SNR penalty, the input power tolerance improved by 8 dB in the 32-channel case and by 10 dB in the 64-channel case. The input power

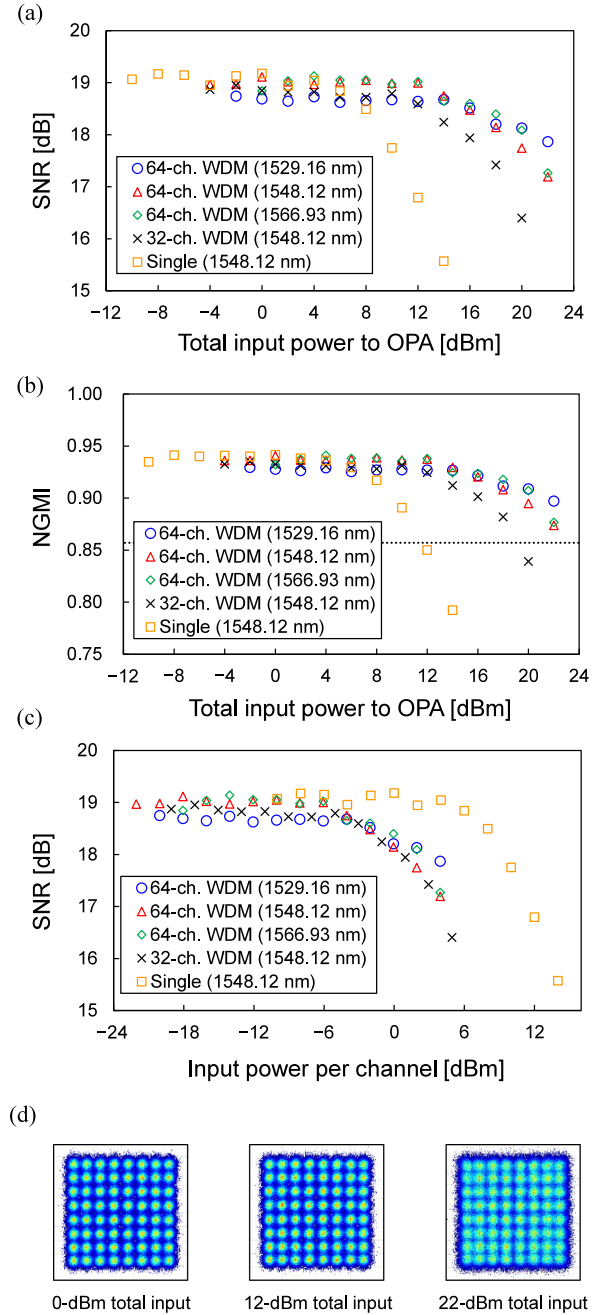


Fig. 14. Input power characteristics of signal distortion in 64-channel and 32-channel WDM cases. (a) SNR characteristics. (b) NGMI characteristics, where dashed line is NGMI threshold for net data rate of 624 Gbps/λ. (c) SNR characteristics for input power per channel. (d) Constellations of demodulated channel at 1548.12 nm in 64-channel case.

of the 64-channel WDM signal for a 1-dB SNR penalty was 18 dBm with a gain reduction of 4.7 dB. We also measured the channel dependence in the 64-channel case, and found that, compared to the center channel (1548.12 nm), the edge channels (1529.16 nm and 1566.93 nm) showed a tolerance improvement of ~1 dB in the range from 14- to 20-dBm input. This result indicates that the wavelength dependence of the effect of the gain saturation on the signal quality is small. A clear difference in constellation was observed at 22-dBm input in the 64-channel

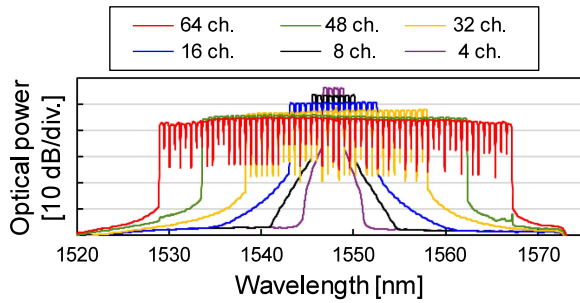


Fig. 15. Output spectra of OPA in each case at total input power of 12 dBm.

case compared to 12-dBm input in the single-channel case, despite a comparable SNR. Distortions dependent on the signal amplitude level were clearly observed in the single-channel case, while a white-like noise was observed in the WDM case. Fig. 14(c) shows the SNR results plotted in terms of power per channel. The 64-channel case and the single-channel case differ in power per channel by ~ 18 dB for the same total input power. The improvement in total input power tolerance thanks to WDM is smaller than the increase in power due to multiplexing, which is why the input power tolerance per channel degraded in the WDM cases. However, the 32- and 64-channel cases showed comparable characteristics despite the 3-dB difference in power per channel for the same total power. These results suggest that the power-per-channel tolerance can be further increased by utilizing a wider bandwidth for OPAs and increasing the number of channels.

We then measured the signal quality at 12-dBm total input by varying the number of WDM channels. Fig. 15 shows the output spectra from the OPA in each case. The channels were increased from around 1548.12 nm and arranged with a high density (75-GHz grid) in all configurations. In other words, an increase in the number of channels corresponded to an increase in the bandwidth of the input WDM signal. Fig. 16 shows the dependence of signal quality on the number of WDM channels. Signal quality improved with increasing the number of channels, and almost no degradation was observed for configurations with 24 channels (1.8 THz) or more. In the 4-channel and 8-channel cases, nonlinear amplitude distortion was visible in the constellation diagrams, while in the 16-channel case, no clear nonlinear distortion could be observed. Fig. 17 shows the spectra of the CUT in the 8-channel and 64-channel cases. To measure the spectrum broadening, adjacent channels of the CUT were cut by the WSS. Total input power was kept at 12 dBm even though the number of channels was reduced for the CUT spectrum measurement. The spectra showed that the spectrum broadening decreased as the number of channels increased. The same as in the single-channel cases, broadening of the spectrum indicates the nonlinear distortion. We presume here that the uncorrelatedness between the electrical field of the WDM signal and the channel is what contributes to the suppression of the nonlinear distortion. The contribution of the time waveform per channel to the overall time waveform of the WDM signal decreases as the number of channels increases. Since the gain saturation of the OPA was caused by the total input power of the WDM signal,

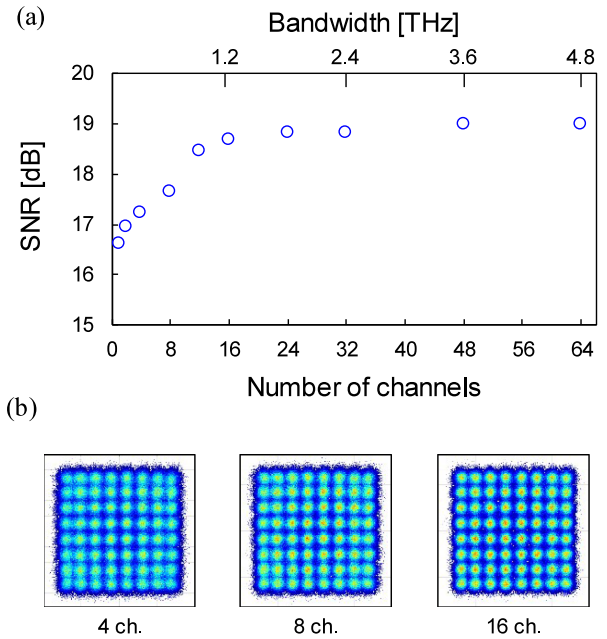


Fig. 16. Signal quality for number of channels. (a) SNR as a function of number and bandwidth. (b) Constellations in 4-ch., 8-ch., and 16-ch. cases. Total input power of WDM signal to OPA was set to 12 dBm in each case.

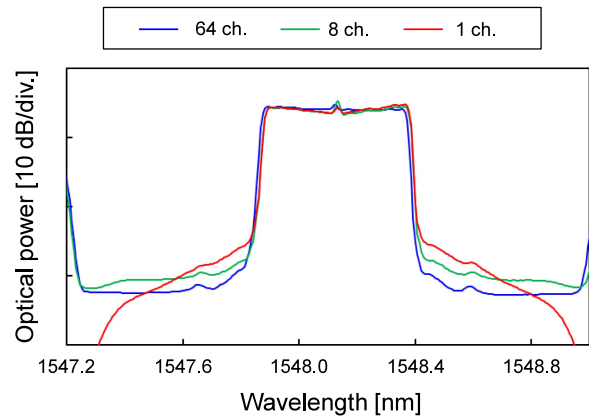


Fig. 17. Amplified spectra in each case. Spectra are parallel shifted so that CUTs overlap for easier comparison of spectral broadening.

the gain reduction occurred randomly on all symbols, not just for particular symbols of the CUT. Therefore, in wideband WDM, the nonlinear distortion was suppressed, and the input power tolerance was improved, despite the increase in PAPR. From this perspective, the variety of frequency distribution in the input signal (i.e., the number of channels) within the amplification band, rather than the signal bandwidth, is the more important factor.

VI. CONCLUSION

We experimentally investigated the effect of the gain saturation in PPLN-based OPA on coherent signals. When the gain saturation for a 64-Gbaud 64QAM signal was converted into a nonlinear signal distortion in the amplitude direction, we found that the distortion was characterized by the PAPR of the input signal in the single-channel case. At the 12-dBm input, the

significant SNR degradation of ~ 2.5 dB was observed. The spectral broadening of the signal also gave a good indication of the nonlinear distortion. We also investigated the effect on a wideband WDM signal and found that, for a 75-GHz-spaced 64-Gbaud 64QAM WDM signal, the SNR penalty due to the nonlinear signal distortion was kept very small for more than 16 channels at a 12-dBm input. At a power resulting in a 1-dB SNR penalty, a total input power tolerance improvement of 10 dB was observed for the 64-channel configuration compared to the single-channel configuration. We also confirmed that there is almost no wavelength dependence of the effect of gain saturation on the signal quality. The power tolerance per channel was degraded, but an increase in the number of WDM channels could relax it. These results demonstrate that PPLN-based OPAs have a wide total input power range for amplifying wideband WDM signals in terms of the nonlinear distortion. As the results obtained in this study were evaluated after only one amplification, future research should examine the cumulative characteristics of multiple passes through the OPAs in a multi-span transmission.

The effect of gain saturation on signal distortion shown in this paper is due to the time waveform of the input signal and the fast response of the optical parametric amplification process, so it would be applicable to OPAs on any platform, not just the PPLN.

ACKNOWLEDGMENT

We thank Mr. Yuto Fujihara for his cooperation in the experiments and fruitful discussions.

REFERENCES

- [1] F. Hamaoka et al., "112.8-Tb/s real-time transmission over 101 km in 16.95-THz triple-band (S, C, and L bands) WDM configuration," in *Proc. 27th Optoelectron. Commun. Conf. Int. Conf. Photon. Switching Comput.*, 2022, pp. 1–3.
- [2] J. Renaudier et al., "First 100-nm continuous-band WDM transmission system with 115Tb/s transport over 100km using novel ultra-wideband semiconductor optical amplifiers," in *Proc. Eur. Conf. Opt. Commun.*, 2017, pp. 1–3.
- [3] L. Galdino et al., "Optical fibre capacity optimisation via continuous bandwidth amplification and geometric shaping," *Photon. Technol. Lett.*, vol. 32, no. 17, pp. 1021–1024, Sep. 2020.
- [4] M. A. Iqbal, L. Krzeczanowicz, I. Phillips, P. Harper, and W. Forsyiaik, "150nm SCL-band transmission through 70km SMF using ultra-wideband dual-stage discrete Raman amplifier," in *Proc. Opt. Fiber Commun. Conf. Exhib.*, 2020, pp. 1–3.
- [5] S. Shimizu et al., "PPLN-based optical parametric amplification for wideband WDM transmission," *J. Lightw. Technol.*, vol. 40, no. 11, pp. 3374–3384, Jun. 2022.
- [6] R. Malik, A. Kumpera, M. Karlsson, and P. A. Andrekson, "Demonstration of ultra wideband phase-sensitive fiber optical parametric amplifier," *Photon. Technol. Lett.*, vol. 28, no. 2, pp. 175–177, Dec. 2015.
- [7] S. Shimizu et al., "Inter-band non-degenerate phase-sensitive amplification scheme for low-noise full C-band transmission," *IEICE Commun. Exp.*, vol. 11, no. 1, pp. 64–69, Jan. 2022.
- [8] C. B. Gaur, V. Gordienko, P. Hazarika, and N. J. Doran, "Polarization insensitive fiber optic parametric amplifier with a gain bandwidth of 22 nm in S-band," in *Proc. Opt. Fiber Commun. Conf. Exhib.*, 2022, pp. 1–3.
- [9] T. Kobayashi et al., "Wide-band inline-amplified WDM transmission using PPLN-based optical parametric amplifier," *J. Lightw. Technol.*, vol. 39, no. 3, pp. 787–794, Feb. 2021.
- [10] T. Kobayashi et al., "50-Tb/s (1 Tb/s \times 50 ch) WDM transmission on two 6.25-THz bands using hybrid inline repeater of PPLN-based OPAs and incoherent-forward-pumped DRA," in *Proc. Opt. Fiber Commun. Conf. Exhib.*, 2022, pp. 1–3.
- [11] C. Guo, A. Shamshooli, Y. Akasaka, P. Palacharla, and M. Vasilyev, "Investigation of hybrid S-band amplifier performance with 8-channel \times 10 GBaud 16-QAM signals," in *Proc. Eur. Conf. Opt. Commun.*, 2021, pp. 1–3.
- [12] T. Kato et al., "Real-time transmission of 240 \times 200-Gb/s signal in S+C+L triple-band WDM without S- or L-band transceivers," in *Proc. 45th Eur. Conf. Opt. Commun.*, 2019, pp. 1–4.
- [13] T. Kato et al., "WDM transmission in S-band using PPLN-based wavelength converters and 400-Gb/s C-band real-time transceivers," in *Proc. IEEE 27th Optoelectron. Commun. Conf. 2022 Int. Conf. Photon. Switching Comput.*, 2022, pp. 1–4.
- [14] T. Kato et al., "S+C+L-band WDM transmission using 400-Gb/s real-time transceivers extended by PPLN-based wavelength converter," in *Proc. IEEE Eur. Conf. Opt. Commun.*, 2022, pp. 1–4.
- [15] H. Kawahara, M. Nakagawa, T. Seki, and T. Miyamura, "Experimental demonstration of wavelength-selective band/direction-switchable multi-band OXC using an inter-band all-optical wavelength converter," in *Proc. IEEE Eur. Conf. Opt. Commun.*, 2020, pp. 1–4.
- [16] G. S. He, *Nonlinear Optics and Photonics*. New York, NY, USA: Oxford Univ. Press, 2014.
- [17] M. Gao, J. Kurumida, and S. Namiki, "Wavelength-tunable optical parametric regenerator," *Opt. Lett.*, vol. 35, no. 20, pp. 3468–3470, Oct. 2010.
- [18] Z. Lali-Dastjerdi et al., "Parametric amplification and phase preserving amplitude regeneration of a 640 Gbit/s RZ-DPSK signal," *Opt. Exp.*, vol. 21, no. 22, pp. 25944–25953, Nov. 2013.
- [19] T. Kobayashi et al., "13.4-Tb/s WDM transmission over 1,280 km repeated only with PPLN-based optical parametric inline amplifier," in *Proc. IEEE Eur. Conf. Opt. Commun.*, 2021, pp. 1–4.
- [20] N. Kamitani, Y. Yoshida, and K. Kitayama, "Experimental study on impact of SOA nonlinear phase noise in 40Gbps coherent 16QAM transmissions," in *Proc. IEEE 38th Eur. Conf. Exhib. Opt. Commun.*, 2012, pp. 1–3.
- [21] J. Renaudier and A. Ghazisaeidi, "Scaling capacity growth of fiber-optic transmission systems using 100-nm ultra-wideband semiconductor optical amplifiers," *J. Lightw. Technol.*, vol. 37, no. 8, pp. 1831–1838, Apr. 2019.
- [22] A. Ghazisaeidi, "Theory of coherent WDM systems using in-line semiconductor optical amplifiers," *J. Lightw. Technol.*, vol. 37, no. 17, pp. 4188–4200, Sep. 2019.
- [23] F. Hamaoka et al., "Experimental investigation of influence of SOA-induced nonlinear distortion on high-symbol-rate 168-GBaud signal for achieving ultra-broadband optical frontend," in *Proc. IEEE Opt. Fiber Commun. Conf. Exhib.*, 2022, pp. 1–3.
- [24] K. Inoue and T. Mukai, "Signal wavelength dependence of gain saturation in a fiber optical parametric amplifier," *Opt. Lett.*, vol. 26, no. 1, pp. 10–12, Jan. 2001.
- [25] K. Inoue and T. Mukai, "Experimental study on noise characteristics of a gain-saturated fiber optical parametric amplifier," *J. Lightw. Technol.*, vol. 20, no. 6, pp. 969–974, Jun. 2002.
- [26] Z. Lali-Dastjerdi, K. Rottwitt, M. Galili, and C. Peucheret, "Asymmetric gain-saturated spectrum in fiber optical parametric amplifiers," *Opt. Exp.*, vol. 20, no. 14, pp. 15530–15539, Jul. 2012.
- [27] L. Jin, A. Martinez, and S. Yamashita, "Optimization of output power in a fiber optical parametric oscillator," *Opt. Exp.*, vol. 21, no. 19, pp. 22617–22627, Sep. 2013.
- [28] K. Inoue, "Analysis of quantum noise of a gain-saturated fiber-based optical parametric amplifier based on an equivalent input noise model," *J. Opt. Soc. Amer. B*, vol. 37, no. 11, pp. 3251–3260, Nov. 2020.
- [29] T. Umeki, T. Kazama, H. Ono, Y. Miyamoto, and H. Takenouchi, "Spectrally efficient optical phase conjugation based on complementary spectral inversion for nonlinearity mitigation," in *Proc. IEEE Eur. Conf. Opt. Commun.*, 2015, pp. 1–3.
- [30] S. Yoshima, Y. Sun, K. R. H. Bottrill, F. Parmigiani, P. Petropoulos, and D. J. Richardson, "Nonlinearity mitigation through optical phase conjugation in a deployed fibre link with full bandwidth utilization," in *Proc. IEEE Eur. Conf. Opt. Commun.*, 2015, pp. 1–3.
- [31] A. D. Ellis et al., "Enhanced superchannel transmission using phase conjugation," in *Proc. IEEE Eur. Conf. Opt. Commun.*, 2015, pp. 1–3.
- [32] K. K. Y. Wong, M. E. Marhic, K. Uesaka, and L. G. Kazovsky, "Polarization-independent one-pump fiber-optical parametric amplifier," *IEEE Photon. Technol. Lett.*, vol. 14, no. 11, pp. 1506–1508, Nov. 2002.
- [33] T. Umeki et al., "PDM signal amplification using PPLN-based polarization-independent phase-sensitive amplifier," *J. Lightw. Technol.*, vol. 33, no. 7, pp. 1326–1332, Apr. 2015.

- [34] V. Gordienko, F. M. Ferreira, C. B. Gaur, and N. J. Doran, "Looped polarization-insensitive fiber optical parametric amplifiers for broadband high gain applications," *J. Lightw. Technol.*, vol. 39, no. 19, pp. 6045–6053, Oct. 2021.
- [35] F. Bessin, V. Gordienko, F. M. Ferreira, and N. Doran, "First experimental Mach-Zehnder FOPA for polarization- and wavelength-division-multiplexed signals," in *Proc. IEEE Eur. Conf. Opt. Commun.*, 2021, pp. 1–3.
- [36] T. Kazama et al., "Over-30-dB gain and 1-dB noise figure phase-sensitive amplification using pump-combiner-integrated fiber I/O PPLN module," *Opt. Exp.*, vol. 29, no. 18, pp. 28824–28834, Aug. 2021.
- [37] T. Kashiwazaki, T. Yamashima, N. Takanashi, A. Inoue, T. Umeki, and A. Furusawa, "Fabrication of low-loss quasi-single-mode PPLN waveguide and its application to a modularized broadband high-level squeezer," *Appl. Phys. Lett.*, vol. 119, 2021, Art. no. 251104.
- [38] T. Kazama, T. Umeki, M. Abe, K. Enbutsu, Y. Miyamoto, and H. Take-nouchi, "Low-parametric-crosstalk phase-sensitive amplifier for guard-band-less DWDM signal using PPLN waveguides," *J. Lightw. Technol.*, vol. 35, no. 4, pp. 755–761, Aug. 2016.
- [39] M. Asobe, T. Umeki, and O. Tadanaga, "Phase sensitive amplification with noise figure below the 3 dB quantum limit using CW pumped PPLN waveguide," *Opt. Exp.*, vol. 20, no. 12, pp. 13164–13172, May 2012.
- [40] R. W. Boyd, *Nonlinear Optics*, 4th ed. Amsterdam, The Netherlands: Elsevier, 2020.
- [41] T. Yanagawa et al., "Simultaneous observation of CO isotopomer absorption by broadband difference-frequency generation using a direct-bonded quasi-phase-matched LiNbO₃ waveguide," *Opt. Lett.*, vol. 31, no. 7, pp. 960–962, Apr. 2006.
- [42] D. H. Jundt, "Temperature-dependent Sellmeier equation for the index of refraction, n_e , in congruent lithium niobate," *Opt. Lett.*, vol. 22, no. 20, pp. 1553–1555, Oct. 1997.
- [43] C. Xie, "Chromatic dispersion estimation for single-carrier coherent optical communications," *IEEE Photon. Technol. Lett.*, vol. 25, no. 10, pp. 992–995, May 2013.
- [44] M. Nakamura, T. Kobayashi, F. Hamaoka, and Y. Miyamoto, "High information rate of 128-GBaud 1.8-Tb/s and 64-GBaud 1.03-Tb/s signal generation and detection using frequency-domain 8×2 MIMO equalization," in *Proc. Opt. Fiber Commun. Conf. Exhib.*, 2022, pp. 1–3.
- [45] R. H. Stolen and C. Lin, "Self-phase-modulation in silica optical fibers," *Phys. Rev. A*, vol. 17, no. 4, pp. 1448–1453, Apr. 1978.
- [46] T. Kobayashi, A. Sano, E. Yamada, E. Yoshida, and Y. Miyamoto, "Over 100 Gb/s electro-optically multiplexed OFDM for high-capacity optical transport network," *J. Lightw. Technol.*, vol. 27, no. 16, pp. 3714–3720, Aug. 2009.

Shimpei Shimizu (Member, IEEE) received the B.E. degree in engineering and the M.E. degree in information science and technology in the field of electronics for informatics from Hokkaido University, Sapporo, Japan, in 2016 and 2018, respectively. In 2018, he joined the NTT Network Innovation Laboratories, Yokosuka, Japan. His research focuses on high-capacity optical transmission systems. He is a Member of the Institute of Electronics, Information and Communication Engineers (IEICE) of Japan and the IEEE Photonics Society. He was the recipient of the 2017 IEICE Communications Society Optical Communication Systems Young Researchers Award.

Takayuki Kobayashi (Member, IEEE) received the B.E., M.E., and Dr. Eng. degrees from Waseda University, Tokyo, Japan, in 2004, 2006, and 2019, respectively. In April 2006, he joined the NTT Network Innovation Laboratories, Yokosuka, Japan, where he was engaged in the research on high-speed and high-capacity digital coherent transmission systems. In April 2014, he moved to the NTT Access Network Service Systems Laboratories, Yokosuka, and was engaged in 5G mobile optical network systems. Since July 2016, he has been with the NTT Network Innovation Laboratories and has been working on high-capacity optical transmission systems. His current research interests include long-haul optical transmission systems employing spectrally efficient modulation formats enhanced by digital and optical signal processing. He is a Member of the Institute of Electronics, Information and Communication Engineers (IEICE) of Japan. From 2016 to 2018, he was a Technical Program Committee (TPC) Member of the Electrical Subsystems' Category for the Optical Fiber Communication Conference (OFC). Since 2018, he has been a TPC Member of the Point-to-Point Optical Transmission Category for the European Conference on Optical Communication (ECOC).

Takushi Kazama received the B.S. and M.S. degrees in electrical engineering from The University of Tokyo, Tokyo, Japan, in 2009 and 2011, respectively. In 2011, he joined the NTT Device Technology Laboratories, Japan, where he has been engaged in research on nonlinear optical devices based on periodically poled LiNbO₃ waveguides. He is a Member of the Institute of Electronics, Information, and Communication Engineers of Japan (IEICE) and the Japan Society of Applied Physics (JSAP).

Masanori Nakamura (Member, IEEE) received the B.S. and M.S. degrees in applied physics from Waseda University, Tokyo, Japan, in 2011 and 2013, respectively, and the Ph.D. degrees in electrical, electronic, and infocommunications engineering from Osaka University, Osaka, Japan, in 2021. In 2013, he joined NTT Network Innovation Laboratories, Yokosuka, Japan, where he engaged in research on high-capacity optical transport networks. He is a Member of the Institute of Electronics, Information and Communication Engineers, Tokyo, Japan. He was the recipient of the 2016 IEICE Communications Society Optical Communication Systems Young Researchers Award.

Akira Kawai received the B.S. and M.S. degrees from the University of Tokyo, Tokyo, Japan, in 2018 and 2020, respectively. In 2020, he joined the NTT Network Innovation Laboratories, Yokosuka, Japan. His research focuses on high-capacity optical transmission systems. He is a Member of the Institute of Electronics, Information and Communication Engineers of Japan.

Koji Enbutsu received the B.E. and M.E. degrees in electronics engineering from Hokkaido University, Sapporo, Japan, in 1994 and 1996, respectively. In 1996, he joined the NTT Opto-Electronics Laboratories, Japan, where he engaged in research on organic optical waveguides for optical communications and electro-optic crystals and their devices. In 2007, he moved to the NTT Access Services Network System Laboratories, where he engaged in research on optical fiber testing and monitoring. He is a Member of the Institute of Electronics, Information, and Communication Engineers and the Japan Society of Applied Physics.

Takeshi Umeki (Member, IEEE) received the B.S. degree in physics from Gakushuin University, Tokyo, Japan, in 2002, and the M.S. degree in physics and the Ph.D. degree in nonlinear optics from The University of Tokyo, in 2004 and 2014, respectively. He joined the NTT Photonics Laboratories, Atsugi, Japan, in 2004, since then he has been involved in research on nonlinear optical devices based on periodically poled LiNbO₃ waveguides. He is a Member of the Japan Society of Applied Physics, the Institute of Electronics, Information, and Communication Engineers, and the IEEE/Photonics Society.

Yutaka Miyamoto (Member, IEEE) received the B.E. and M.E. degrees in electrical engineering from Waseda University, Tokyo, Japan, in 1986 and 1988, respectively, and the Dr. Eng. degree in electrical engineering from Tokyo University, Tokyo, in 2016. In 1988, he joined the NTT Transmission Systems Laboratories, Yokosuka, Japan, where he was engaged in the research and development of high speed optical communications systems, including the 10-Gbit/s first terrestrial optical transmission system (FA-10G) using erbium-doped fiber amplifiers (EDFA) inline repeaters. From 1995 to 1997, he was with the NTT Electronics Technology Corporation, Yokohama, Japan, where he was engaged in the planning and product development of high-speed optical module at the data rate of 10 Gb/s and beyond. Since 1997, he has been with the NTT Network Innovation Laboratories, Yokosuka, where he has contributed to the research and development of optical transport technologies based on 40/100/400-Gbit/s channel and beyond. He is currently an NTT Fellow and the Director of the Innovative Photonic Network Research Center, NTT Network Innovation Laboratories, where he has been investigating and promoting the future scalable optical transport network with the Pbit/s-class capacity based on innovative transport technologies, such as digital signal processing, space division multiplexing, and cutting-edge integrated devices for photonic preprocessing. He is a Fellow of the Institute of Electronics, Information and Communication Engineers.